International Journal of Applied Engineering Research ISSN 0973-4562 Volume 11, Number 11 (2016) pp 7415-7419

Influence of Surface Tension on Shapes of Air Taylor Bubbles in Stagnant Liquids under Laminar Conditions in Falling-Film Regions

Boonchai Lertnuwat
Department of Mechanical Engineering, Chulalongkorn University
254 Phaya Thai Rd., Wang Mai, Pathum Wan, Bangkok 10330, Thailand.

Abstract
The objective of this work is to numerically investigate how a shape of an air Taylor bubble in a stagnant liquid changes when the surface tension of the interface between gas and liquid is varied. Five examined surface tensions are chosen between 6 and 10 N/m so that all the flows around a Taylor bubble are entirely laminar. The Taylor bubble shape is adjusted until a proper shape is found by considering a pressure distribution of the air inside the bubble. This is obtained from a program code, developed from the implicit pressure-correction method on the finite volume framework with second order spatial accuracy. Simulation results finally show that the Taylor bubble shape will be slenderer if the surface tension is smaller because of the influence of the surface tension on Froude number. Additionally, it is also found that all the Taylor bubble shapes in this work are slenderer than that created by Dumitrescu's model.

Index Terms: Dumitrescu's model, Laminar, Surface Tension, Taylor bubble

INTRODUCTION & THEORY

The slug flow, shown in Figure 1 (a), is a type of gas-liquid flows. Numerically, the behavior of the slug flow is often studied by considering the flow as a unit, comprised of a Taylor bubble, a liquid slug and a falling film. The flow in the slug flow unit is considered with respect to the Taylor bubble nose as shown in Figure 1 (b). In this figure, the velocity magnitude of the liquid (w_l) is equal to the rising velocity of a Taylor bubble in a vertical pipe (w_b) in Figure 1 (a) but its direction is opposite to that of w_b. When the liquid is stagnant, the magnitude of

$$w_b = w_t = Fr_D\sqrt{gD_p} \ . \qquad (1)$$

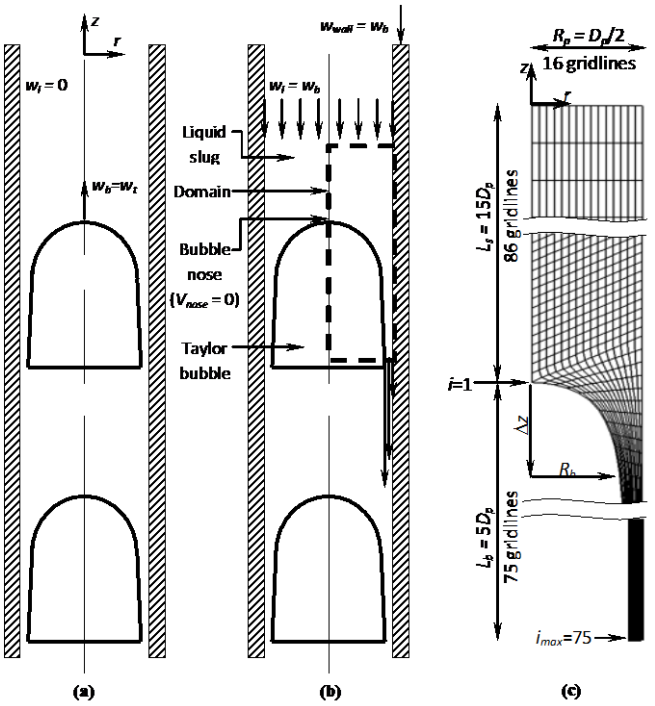

Figure 1: Schematic diagrams of slug flows in stagnant liquids (a) with respect to pipe wall (b) with respect to Taylor bubble nose and (c) the computational domain and exploited grid

Hayashi et al. [1] used the data obtained from a work of White and Beardmore [2] to develop a formula to estimate the Fr_D in Eq. (1) under intermediate Morton numbers and proposed that

$$Fr_D = \sqrt{\frac{0.0089}{0.0725 + \frac{\mu_l}{\rho_l Fr_D\sqrt{gD_p^3}}\left(1 - 0.11\left(\frac{\rho_l Fr_D\sqrt{gD_p^3}}{\mu_l}\right)^{0.33}\right)}\left(1 + 41\left(\frac{\sigma}{(\rho_l - \rho_g)gD_p^2}\right)^{1.96}\right)^{-4.63}} \ . \qquad (2)$$

The above equation reveals that the Fr_D will be a function of only σ if ρ_g , ρ_l , μ_l and D_p are fixed. Since air-water slug flows are often studied in many researches, the properties of examined fluids are assumed to be ρ_g =1.18 kg/m^3 and ρ_l =1000 kg/m^3 and μ_l = 0.0010 Pa-s. The D_p is set to be 0.05 m, which is approximately the average diameter of pipe, in which air Taylor bubbles rising in stagnant water are found in accordance with some former works ([3]-[10]).

Mayor et al. [11] stated that the flow field around a Taylor bubble would be entirely laminar when Re_{film} is less than 250. Herein,

$$Re_{film} = \frac{\rho_l \bar{w}_{film} \delta_{film}}{\mu_l} \approx \frac{\rho_l w_t D_p}{4\mu_l}. \quad (3)$$

If the turbulence influence need to be eliminated, the minimum σ will be greater than 5.20 N/m in accordance with Eq. (2) and Eq. (3). Hence, 5 values of σ are selected as listed in Table 1 in order to investigate the influence of σ on the shape of the Taylor bubble when the flow in the falling film is laminar.

Table 1: Values of parameters for 5 investigating conditions

σ (N/m)	w_l (m/s)	Fr_D $(w_b/\sqrt{gD_p})$	Re_{film} $(\frac{\rho_l w_t D_p}{4\mu_l})$	Eo_D $(\frac{[\rho_l-\rho_g]gD_p^2}{\sigma})$	M $\{\frac{[\rho_l-\rho_g]g\mu_l^4}{\rho_l^2\sigma^3}\}$
6.00	1.267 $\times 10^{-2}$	1.809 $\times 10^{-2}$	158.36	4.09	1.64 $\times 10^{-15}$
7.00	7.468 $\times 10^{-3}$	1.066 $\times 10^{-2}$	93.35	3.50	1.40 $\times 10^{-15}$
8.00	4.572 $\times 10^{-3}$	6.529 $\times 10^{-3}$	57.15	3.07	1.23 $\times 10^{-15}$
9.00	2.895 $\times 10^{-3}$	4.134 $\times 10^{-3}$	36.19	2.73	1.09 $\times 10^{-15}$
10.00	1.886 $\times 10^{-3}$	2.692 $\times 10^{-3}$	23.57	2.45	0.98 $\times 10^{-15}$

METHODOLOGY & COMPUTATIONAL SETUP

The employed program code is given in [12]. The computational method, used in the program code, is the implicit pressure-correction method on the finite volume framework with second order spatial accuracy. Figure 1 (b) shows dash lines, confining a computational domain. The domain occupies just on the right side of the pipe because simulated flows are assumed to be symmetric along the pipe centerline. According to some literature reviews ([5], [6], [13] and [14]), the average value of the slug length (L_s) equals $15\,D_p$ and the Taylor bubble length (L_b) equals $5\,D_p$ as shown in Figure 1 (c). There are 16 gridlines on the r-axis. Whereas the gridlines on the z-axis are divided in 2 parts, i.e. 86 gridlines are drawn from the centerline of the pipe and 75 gridlines are drawn from the Taylor bubble surface. This is the same grid system, used in [15]. In this work, a velocity inlet boundary condition is posed on the top of the domain with a fixed velocity (w_l) shown in Table 1, depending on the investigating condition. A pressure outlet condition is posed on the bottom of the domain with a fixed constant (p_l =100kPa). A no-slip condition is posed along the pipe wall on the right side of the domain with a fixed wall velocity ($w_{wall} = w_l$). A symmetry boundary condition is posed along the pipe centerline on the upper left side of the domain. And a free surface boundary condition is posed along the Taylor bubble surface on the lower left side of the domain. According to the work of Lertnuwat [16], shapes of the Taylor bubble surface (R_b) are created with

$$\frac{R_b}{D_p} = \frac{1}{2}\left[1-\left(\frac{\beta w_b^2+\delta}{2g\Delta z+\delta}\right)^{\frac{1}{2}}\right]^{\frac{1}{2}}, \quad (4)$$

$$\beta = a_1\left(1-e^{a_2\Delta z/D_p}\right), \quad (5)$$

$$\Delta z = z_{nose} - z. \quad (6)$$

in which δ is a small constant (assigned to be 10^{-38}) and added in order to avoid a singular point at $\Delta z = 0$. In accordance with Eq. (4) and Eq. (5), shapes of the Taylor bubble can be adjusted with the values of α_1 and α_2 if D_p is specified.

After each case of the flow simulation is complete, a pressure distribution of liquid along the Taylor bubble surface will be known. Next, the liquid pressure at each grid vertex along the outside surface of the Taylor bubble will be used to calculate a gas pressure inside the Taylor bubble as follows

$$p_g\big|_{bs} = p_l\big|_{bs} + \sigma\frac{1}{R_{bs}} - 2\mu_l\left(\frac{\partial V_n}{\partial n}\right)_l\Bigg|_{bs}. \quad (7)$$

The symbol (R_{bs}) is a radius of curvature, which is defined as

$$\frac{1}{R_{bs}} = \frac{1}{R_{bs1}} + \frac{1}{R_{bs2}} \quad (8)$$

where

$$R_{bs1} = -\left[1+\left(\frac{\partial z}{\partial r}\right)^2\right]^{\frac{3}{2}}\Bigg/\frac{\partial^2 z}{\partial r^2} \text{ and } R_{bs2} = r\left[1+\left(\frac{\partial r}{\partial z}\right)^2\right]^{\frac{1}{2}}.$$

Since, ideally, the distribution of the gas pressure inside a Taylor bubble must be uniform, the values of α_1 and α_2 must be varied to adjust the Taylor bubble shape until the uniform distribution of the gas pressure inside a Taylor bubble is achieved. For the sake of simplicity, the root-mean-square derivation ($RMSD$) of residuals between the gas pressure at each grid vertex along the Taylor bubble surface ($p_{g,i}\big|_{bs}$) and the gas pressure at the Taylor bubble nose ($p_{g,nose}\big|_{bs}$), i.e.

$$RMSD_p = \sqrt{\left[\sum_{i=1}^{i_{\max}}\left(p_{g,i}\big|_{bs} - p_{g,nose}\big|_{bs}\right)^2\Big/\left(i_{\max}-1\right)\right]}, \quad (9)$$

is used to numerically indicate how a pressure distribution, obtained from a simulation, is close to the ideal pressure distribution. The location $i=1$ is the location of the Taylor bubble nose. And the $i_{\max}$ is the number of the data point along the Taylor bubble surface, namely $i_{\max}=75$ as shown in Figure 1 (c). Apparently, $RMSD_p$ will become zero if the considered pressure distribution is ideally uniform. However, the uniform pressure distribution is in practice difficult to be obtained so the minimum $RMSD_p$ is an alternative which can be found by using the grid search method. At first, a coarse grid with large values of $\Delta\alpha_1$ and $\Delta\alpha_2$ is used. Once the

first-round searching is finished, approximately proper values of α_1 and α_2, which give minimum $RMSD_p$, will be known. Then, a finer grid is employed to determine more accurate values of α_1 and α_2. The procedure of using finer grids will be repeated until a required accuracy of α_1 and α_2 is obtained. During the searching procedure, values of α_1 and α_2 that create spiky-nose Taylor bubbles will be eliminated because they are unnatural.

RESULTS

Table 2 shows appropriately proper values of α_1 and α_2, obtained from the simulations for each σ. While σ slightly increases, the value of α_1 dramatically increases but the value of α_2 slightly decreases.

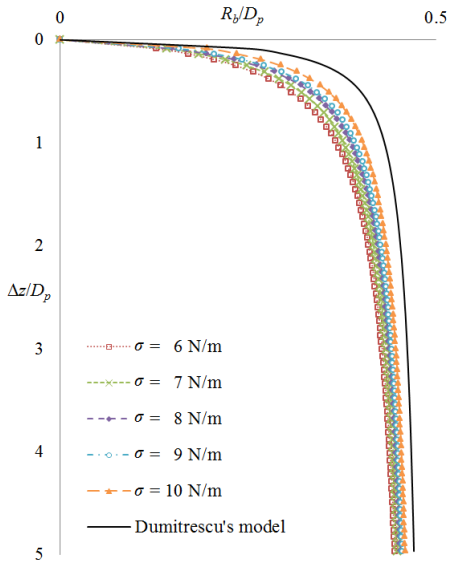

(a) Whole body

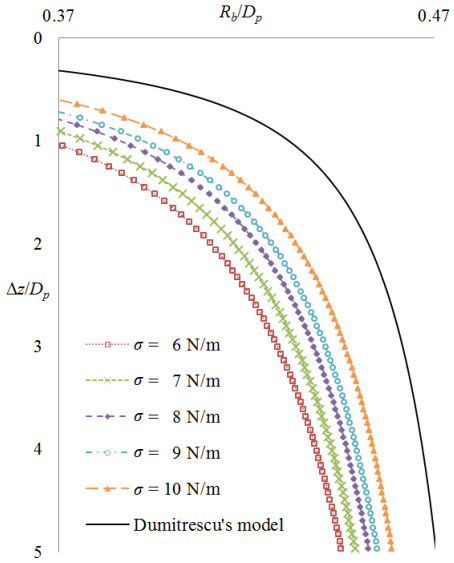

(b) Wall region

Figure 2: Influence of σ on shapes of air Taylor bubbles in stagnant water

Substituting the values of α_1 and α_2 in Table 2 into Eq. (4) and Eq. (5) will give us the appropriate shape of a Taylor bubble for each σ. Figure 2 (a) shows a comparison among the appropriate shapes of Taylor bubbles, which are made to be dimensionless with D_p, so that the comparison is easier. The comparison reveals that the dimensionless shape of a Taylor bubble is slenderer when σ is smaller. This will be clearer if the wall region is enlarged as shown in Figure 2 (b). The result agrees well with a result in [17], namely when σ decreases, both Eo_D and M increase but the Taylor bubble shape is slenderer. Besides Figure 2 (b) shows the dimensionless shape of the Taylor bubble obtained from Dumitrescu's model [18], i.e.

$$R_b = R_p\left[\frac{\Delta z}{R_p}\left(\frac{3}{2}-\frac{\Delta z}{R_p}\right)\right]^{\frac{1}{2}} \text{ when } \Delta z \le 0.5R_p, \qquad (10)$$

$$R_b = R_p\left[1-(0.351)\left(\frac{R_p}{\Delta z}\right)^{\frac{1}{2}}\right]^{\frac{1}{2}} \text{ when } \Delta z > 0.5R_p. \qquad (11)$$

These equations were proposed in [3]. The comparison shows that Dumitrescu's model gives the thickest shape of the Taylor bubble. This is consistent with the results, found in [3], too.

Table 2: Appropriate values of α_1 and α_2 for each σ

σ (N/m)	α_1	α_2
6.00	1300	-5.1
7.00	3280	-5.8
8.00	7640	-6.8
9.00	17300	-7.5
10.00	34300	-8.1

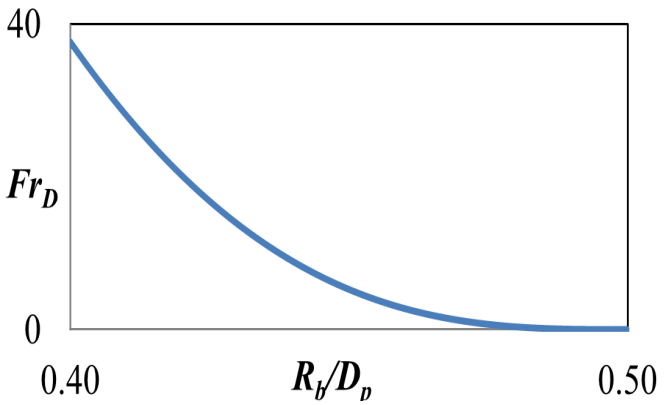

Figure 3: The relation between R_b/D_p and Fr_D.

DISCUSSION

The reason why σ affects the shape of a Taylor bubble possibly can be clarified by considering the liquid flow in the region of the falling film. Since the liquid flow in the falling film are laminar due to the sufficiently low Re_{film} for all

investigating conditions, the velocity profile in a fully developed falling film may be written as ([3], [15] and [19])

$$w_l = w_{wall} + \frac{\rho_l g R_p^2}{4\mu_l}\left[1 - \frac{r^2}{R_p^2} + 2\frac{R_b^2}{R_p^2}\ln\left(\frac{r}{R_p}\right)\right]. \quad (12)$$

By applying a mass-flux balance between the inlet plane far ahead of the Taylor bubble and a plane located at the fully developed film, with respect to a reference frame, which is moving with the bubble as shown in Figure 1 (b), we get

$$\int_{R_b}^{R_p} \rho\left[2\pi r w_l\right]dr = \rho w_t \pi\left(R_p^2\right). \quad (13)$$

Substituting Eq. (12) into Eq. (13) yields

$$\frac{1}{32}\left[48\left(\frac{R_b}{D_p}\right)^4 - 64\left(\frac{R_b}{D_p}\right)^4 \ln\left(\frac{2R_b}{D_p}\right) - 16\left(\frac{R_b}{D_p}\right)^2 + 1\right] = \frac{\mu_l}{\rho_l g^{1/2} D_p^{3/2}} Fr_D. \quad (14)$$

In case that μ_l, ρ_l, g and D_p are fixed, Eq. (14) can be used to depict a relation between R_b/D_p and Fr_D as a graph in Figure (3). Herein, Fr_D will increase if R_b/D_p decreases, that is the shape of a Taylor bubble is slenderer. In accordance with Table 1, it shows that Fr_D will increase if σ decreases. Owing to these 2 relations, it thus can be concluded that the shape of a Taylor bubble will be slenderer if the value of σ is decreased. This explanation can also be applied to the shape of a Taylor bubble, created by Dumitrescu's model, which is derived from the potential flow theory. As we know that potential flows are assumed to be inviscid (μ_l = 0) so the value of the right-hand-side of Eq. (14) will be zero. As a result, R_b/D_p will become 0.5, leading to the thickest shape of a Taylor bubble as shown in Figure 2.

CONCLUSION

The surface tension of the interface between an outside liquid and an inside gas of a Taylor bubble can affect the shape of the Taylor bubble in stagnant water. If only σ is reduced, the Taylor bubble will be slenderer. This could be explained with the velocity profiles around the Taylor bubble. The appropriate shape of the Taylor bubble can be created by using Eq. (4) and Eq. (5) with the values of α_1 and α_2, given in Table 2. Furthermore, it is found that all the shapes of Taylor bubbles in this work are slenderer than that created by the Dumitrescu's model due to the effect of the liquid viscosity.

However, a limitation of applying the proposed model is found when the proposed model is used to predict the shape of a Taylor bubble nose with a very small value of $\Delta z/D_p$, i.e. when $0 < \Delta z/D_p < 0.04$, the proposed model will give imaginary numbers. Hence, interpolation may be applied in this narrow interval with an acceptable error.

ACKNOWLEDGEMENT

This research was supported by CHULA-ISUZU Funding, Faculty of Engineering, Chulalongkorn University.

NOMENCLATURE

Characters

D	Pipe diameter
Eo	Eötvös number
Fr	Froude number
g	Acceleration of gravity
M	Morton number
n	Unit normal
p	Static pressure
R	Radius or Radius of curvature
Re	Reynolds number
$RMSD$	Root-mean-square deviation
u	Velocity component on r-axis
V	Total velocity
w	Velocity component on z-axis

Symbols

Δz	Distance from bubble nose
σ	Surface tension

Superscripts and Subscripts

b	Taylor bubble
bs	Taylor bubble surface
$film$	Falling film
g	Gas
l	Liquid
$nose$	Taylor bubble nose
p	Pipe
s	Slug
t	Terminal

REFERENCES

[1] Hayashi, K., Kurimoto, R., and Tomiyama, A., 2011, "Terminal Velocity of a Taylor Drop in a Vertical Pipe," Int. J. Multiphase Flow, 37, pp. 241-251.

[2] White, E. T., and Beardmore, R. H., 1962, "The Velocity of Rise of Single Cylindrical Air Bubbles through Liquids Contained in Vertical Tubes," Chem. Eng. Sci., 17(5), pp. 351-361.

[3] Nogueira, S., Riethmuler, M. L., Campos, J. B. L. M., and Pinto, A. M. F. R., 2006, "Flow in the Nose Region and Annular Film Around a Taylor Bubble Rising through Vertical Columns of Stagnant and Flowing Newtonian Liquids," Chem. Eng. Sci., 61, pp. 845-857.

[4] Ahmad, W. R., DeJesus, J. M., and Kawaji, M., 1998, "Falling Film Hydrodynamics in Slug Flow," Chem. Eng. Sci., 53, pp. 123-130.

[5] Mao, Z. S., and Dukler, A. E., 1991. "The Motion of Taylor Bubbles in Vertical Tubes-II. Experimental Data and Simulations for Laminar and Turbulent flow," Chem. Eng. Sci., 46(8), pp. 2055-2064.

[6] Hout, R. V., Bernea, D., and Shemer, L., 2001, "Evolution of Statistical Parameters of Gas-Liquid

Slug Flow along Vertical Pipes," Int. J. Multiphase Flow, 27, pp. 1579-1602.

[7] Pinto, A. M. F. R., Coelho Pinheiro, M. N. and Campos, J. B. L., 2001, "On the Interaction of Taylor Bubbles Rising in Two-Phase Co-Current Slug Flow in Vertical Columns: Turbulent Wakes," Experiments in Fluids, 31, pp. 643-652.

[8] Kytömaa, H. K., and Brennen, C. E., 1991, "Small Amplitude Kinematic Wave Propagation in Two-Component Media", Int. J. Multiphase Flow, 17(1), pp. 13-26.

[9] Cheng, H., Hills, J. H., and Azzorpardi, B. J.,1998, "A Study of the Bubble-to-Slug Transition in Vertical Gas-Liquid Flow in Columns of Different Diameter," Int. J. Multiphase Flow, 24(3), pp. 431-452.

[10] Sun, B., Wang, R., Zhao, X., and Yan, D., 2002, "The Mechanism for the Formation of Slug Flow in Vertical Gas-Liquid Two-Phase Flow," Solid State Electron. 46(12), pp. 2323-2329.

[11] Mayor, T. S., Pinto, A. M. F. R., and Campos, J. B. L. M., 2007, "Hydrodynamics of gas-liquid slug flow along vertical pipes in the laminar regimes-experimental and simulation study," Ind. Eng. Chem. Res., 46, pp. 3794-3809.

[12] Ferziger, J. H., and Peric, M., 2002, Computational Methods for Fluid Dynamics, third ed., Springer, Germany.

[13] Hout, R. V., Bernea, D., and Shemer, L., 2003, "Evolution of Hydrodynamic and Statistical Parameters of Gas-Liquid Slug Flow along Inclined Pipes," Chem. Eng. Sci., 58, pp. 115-133.

[14] Shemer, L., 2003. "Hydrodynamic and Statistical Parameters of Slug Flow," Int. J. Heat Fluid., 24, pp. 334-344.

[15] Lertnuwat, B., Angariya, N., Chaokijka, W., and Nuchjaroen, P., 2014, "Influence of Pipe Diameters on Shapes of Air Taylor Bubbles in Small Pipes Containing Stagnant Water", Applied Mechanics and Materials, 619, pp. 18-22.

[16] Lertnuwat, B, 2015, "Model for Predicting the Head Shape of a Taylor Bubble Rising through Stagnant Liquids in a Vertical Tube," Thammasat International Journal of Science and Technology, 20(1), pp. 37-46.

[17] Bugg, J. D., Mack, K., and Rezkallah, K. S., 1998, "A Numerical Model of Taylor Bubbles Rising through Stagnant Liquids in Vertical Tubes," Int. J. Multiphase Flow, 24(2), pp. 271-281.

[18] Dumitrescu, D. T., 1943, "Strömung an Einer Luftblase im Senkrechten Rohr," Zeitschrift fur Angewandte Mathematik und Mechanik, 23, pp. 139-149.

[19] Thulasidas, T. C., Abraham, M. A., and Cerro, R. L., 1995, "Bubble-Train Flow in Capillaries of Circular and Square Cross Section," Chem. Eng. Sci., 50, pp. 183-199.